Automated detection and mapping of electrical activation when electrogram morphology is complex

Ernesto F. Treo [a], Daniel O. Cervantes [b], Edward J. Ciaccio [c],*

[a] Departamento de Bioingeniería, Universidad Nacional de Tucumán, Argentina
[b] Department of Pharmacology, Columbia University, New York, USA
[c] Department of Medicine – Division of Cardiology, Columbia University, New York, USA

ARTICLE INFO

ABSTRACT

Background: Mapping of cardiac electrical activity can be difficult when electrogram morphology is complex. Complex morphology (multiple and changing deflections) causes activation maps to vary when constructed by different analysts, particularly at areas with spatially varying conduction pattern. An algorithm was developed to automatically detect electrogram activation time which is robust to complex morphology.

Method: Electrograms, many of which were complex, were collected from 320 canine epicardial border zone sites in five experiments. A library of electrogram activation times were manually marked a priori by two expert analysts. Then an algorithm which combined correlation and error functions was used to compare each input electrogram to library electrogram patterns. The closest match of input to library electrogram was used to estimate activation time. Once activation times at 320 sites were determined, activation maps were automatically constructed on a computerized grid. The algorithm was validated by comparison with activation times determined by the analysts.

Results: The mean difference between manual and automated marking of activation time in electrograms acquired during reentrant ventricular tachycardia was 2.1 ± 3.9 ms. The mean sensitivity and positive predictive value were 95.9% and 83.8% respectively. The computer-automated marking process was completed within a few seconds and was robust to fractionated electrograms. Measurement error was mostly attributable to 60 Hz noise, which can be rectified with filtering.

Conclusions: The automated algorithm is useful for rapid and accurate automatic marking of multichannel electrograms, some of which may be fractionated, as well as for real-time display of activation maps in clinical electrophysiology or research studies.

© 2012 Elsevier Ltd. All rights reserved.

1. Introduction

Electrical activation mapping is widely used in clinical electrophysiologic study to assist in diagnosis and treatment of cardiac rhythm disorders [1], during the testing of antiarrhythmic drugs [2] and for detection of heart arrhythmias [3]. Although many types of cardiac mapping devices are known [4], most of them require the storage of large volumes of data which is processed manually, with the results displayed as isochronal maps [5–8]. Yet for accurate analysis, the spatial resolution of multichannel electrodes should be high (2–5 mm). Manual marking of complex fractionated electrograms for activation time, or even automated marking with manual correction, is time-consuming, particularly

when multiple cardiac cycles require marking and mapping. Yet it is these electrograms that are most often pertinent for identifying arrhythmogenic regions. Thus, accurate activation mapping during electrophysiologic study in real or near-real time can be difficult.

Automated algorithms for recognition and processing of heart signals are commonly tested with standard databases [9]. These algorithms, mostly intended to recognize ectopic beats and arrhythmogenic processes [10], have limited utility in heart surface cardiac mapping. Besides the increased likelihood of fractionated waveforms appearing in surface recordings in remodeled tissues, particularly when recorded during tachyarrhythmias, the time of all electrical activation points must be determined precisely to accurately detect complex activation patterns [11]. It is even more difficult to identify activation times during fibrillation, although template matching methods have been used with some success [12,13]. However, when complex electrical activity causes time-varying polyphasic electrogram deflections, and is of variable duration, template matching is often not satisfactory [14]. Another

* Corresponding author at: Harkness Pavilion 804, Columbia University Medical Center, 180 Fort Washington Avenue, New York, NY 10032, USA.
Tel.: +1 212 305 5447; fax: +1 212 342 0447.
E-mail address: ciaccio@columbia.edu (E.J. Ciaccio).

difficulty of automated marking is the fact that poor electrode contact can cause additive noise and motion artifact.

To overcome these limitations, an algorithm was developed to rapidly determine activation time and to display activation maps from multichannel electrogram data. The automated algorithm correlates small segments of the acquired electrograms to a set of library patterns. In this study, a statistical analysis of the method as compared with manual marking is done, and the affect of the signal-to-noise ratio on algorithm performance is discussed.

2. Methods

2.1. Data acquisition

In mongrel dogs anesthetized with 30 mg/kg of sodium pentobarbital and having a weight of 20–40 kg, the left anterior descending coronary artery (LAD) was surgically ligated near its origin [15]. Three to five days post-LAD ligation, the same anesthetic was administered and the animals were prepared for electrophysiologic analysis by applying positive pressure ventilation and opening the chest cavity, exposing the heart through a midsternal opening. A 312 bipolar electrode array with 3–5 mm spatial resolution and 1 mm spacing between bipoles was sutured to the anterior left ventricle over the epicardial border zone, the narrow rim of surviving myocardium on the epicardial surface of the healing infarct. In each experiment, the array approximately overlapped the entire epicardial border zone, as could be ascertained by noting the color of the heart surface and by electrogram characteristics. Electrogram signals of 5 s duration were amplified 100–1000×, bandpassed from 1 to 500 Hz, sampled at 1 kHz, and recorded on archival media along with electrocardiogram, stimulus channel and blood pressure [16]. Following each experiment, the data were analyzed using PC-computer software programs that were developed by the authors. Monomorphic VT was initiated using programmed electrical stimulation from electrodes positioned at the border zone margins or from its center, using twice the current threshold required for a propagated response. The pace train for induction consisted of ten S1–S1 stimuli, each of 2 ms duration, that were separated by approximately 300 ms intervals, and were followed by a single extrastimulus S2 of 2 ms duration. The S1–S2 coupling interval was decreased by 5–10 ms during each sequence until monomorphic ventricular tachycardia was induced or a propagated response was not initiated. Monomorphic ventricular tachycardia episodes were often repeatedly induced by the same procedure and included nonsustained runs (<30 s duration), and sustained episodes which were pace-terminated (>30 s duration). Use of canines conformed to the guidelines of the American Physiological Society and AAALAC.

2.2. Activation marking and mapping

Bipolar electrograms were manually marked for activation time by two experts based on morphology, by selecting the sharpest slope associated with a large peak deflection, so that timing would be similar to that of electrically contiguous nearby recording sites [15,16]. The experts were electrophysiologists with at least 2 years' experience in manual activation marking and mapping. It has been shown that when bipolar electrograms are marked, morphological algorithms produce fewer anomalous activation times as compared with peak and fastest zero crossing techniques [17]. Marks in agreement within 5 ms were used for further analysis, with the marking times for the two experts being averaged. The activation times were mapped on a computerized grid. On these grids, individual activation times could be displayed, as well as isochronal lines of activation with 10–20 ms spacing. Lines of block were considered to occur at boundaries where activation on either side was

dyssynchronous by $\geq$40 ms and the activation wavefront propagated in different directions. The reentry isthmus location during monomorphic ventricular tachycardia, its functional block lines, and entrance and exit point locations were determined.

In previous work, the mean squared error difference between an input electrogram and a prototypical or template electrogram (extracted from the first cardiac cycle in the sequence) was used for comparison [18,19]. Yet, this method can be sensitive to outliers due to the quadratic term. Digital correlation, which is less sensitive to outliers caused by large differences in signal shape [20,21], was utilized in the present study to compare library template to input. A problem with digital correlation however is that the typical correlation signal can present sidelobes, or local maxima, due to overlap of template peaks to non-corresponding peaks in the input electrogram. This phenomenon can make it difficult to identify the global maxima representing the correct match of electrogram input to template. If for example the electrogram is fractionated or otherwise multiphasic, the relative relationship between peak amplitudes may change from one cardiac cycle to the next. The effect is that maximum correlation can occur when multiphasic peaks of input and template are aligned with the wrong counterpart. To reduce this potentially large source of error, a measure of the degree of overlap in the input to the template trace is needed [22]. This was done as follows. Consider an electrogram input $x(n)$ and a template pattern $y(n)$, then:

$$r_{xy}(i) = \ell^{-1} \cdot \sum x(n+i) \cdot y(n) \quad \text{for } n = 1, \ldots, \ell, \ i = 1, \ldots, s \quad (1)$$

and

$$e_{xy}(i) = \ell^{-1} \cdot \sum |x(n+i) - y(n)| \quad \text{for } n = 1, \ldots, \ell, \ i = 1, \ldots, s \quad (2)$$

where $r_{xy}(i)$ and $e_{xy}(i)$ are, respectively, the correlation and the absolute error signal between the electrogram x and pattern y, ℓ is the pattern duration, and s is the sequence length of the input signal. As the error and correlation are evaluated for sample i, the pattern will be matched within the interval $[i, i+s]$ of the electrogram. If input and template are similar, maxima in $r_{xy}(i)$ (i.e., when correlation is maximized) will coincide with minima in $e_{xy}(i)$ (when the degree of overlap of template and input electrogram is maximized). Peaks in the correlation signal as described by Eq. (1) were used to identify candidate activation times. The value of the absolute error, given by Eq. (2), served to estimate the similarity of template to input. If template and input are similar (nearly overlapping) then the value of $e_{xy}(i)$ will be small. Activation was considered to occur at points where $r_{xy}(i)$ peaked and $e_{xy}(i)$ was below a threshold level. The threshold level was determined heuristically by training with an exemplar set of electrograms to approximately maximize the sensitivity of the method. The threshold was set to approximately 10% of the mean absolute value of the input. Once an activation point was detected, an adjustment in time t served to align the correlation peak with the actual time of local activation in each library template, as determined prior to implementation.

2.3. Automated activation marking algorithm

Each input electrogram was preprocessed as follows before estimating the activation time: the electrogram was normalized by setting the average (baseline) level to zero and adjusting the peak-to-peak amplitude to 1 mV. Fig. 1 shows an arbitrary input electrogram $x(n)$, and its result after normalization $x_{\text{nor}}(n)$ which is shown in the second row. This does not change the intrinsic shape, but only the shift and scale along the y-axis. The correlation of input electrogram with an arbitrary template of length ℓ sample points is shown in the third row in Fig. 1 and is termed Corr(n),
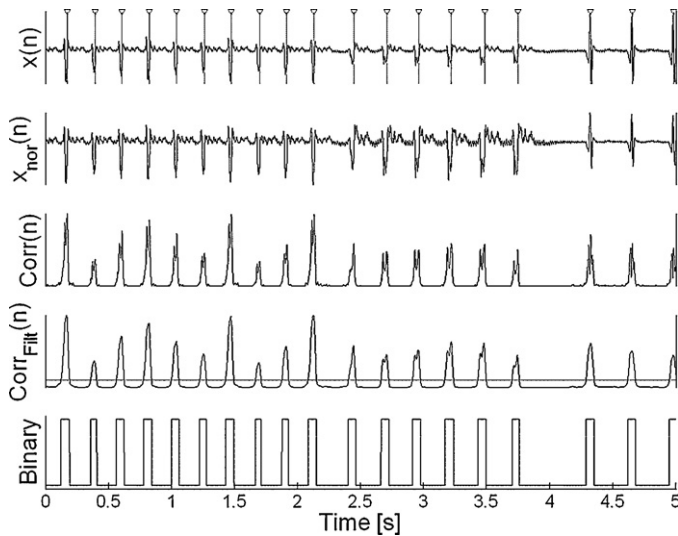
Fig. 1. Computation of the correlation signal. Electrogram $x(n)$ and its normalized version $x(n)_{nor}$, the correlation signal Corr(n) and its filtered version Corr(n)$_{filt}$ are shown. Corr(n)$_{filt}$ is converted to a binary signal (bottom trace). Maxima in Corr(n) within binary 1 (high level) are used as activation marks, denoted by the gray vertical lines in $x(n)$.

which is then low pass filtered to remove local extrema, forming Corr$_{Filt}(n)$, shown in the fourth row. The low pass filter was a Hamming window finite impulse response (FIR) with 28 coefficients, and had a corner frequency, determined heuristically, of 19.5 Hz. The Corr$_{Filt}(n)$ signal was then transformed to a binary signal using thresholding (lowest trace in Fig. 2). The threshold T utilized was:

$$T = 0.5 \times \mathrm{MA}\left[P_{\mathrm{CorrFilt}}(n)\right] \tag{3}$$

where MA is the moving average and P are the peak values of the filtered correlation signal. Thus prior detected peak amplitudes are used to form the moving average. The estimated activation time was defined as the time of raw correlation signal maximum during the interval binary 1. Since the binary 1 interval extended across the base of each major electrogram deflection, the slight phase
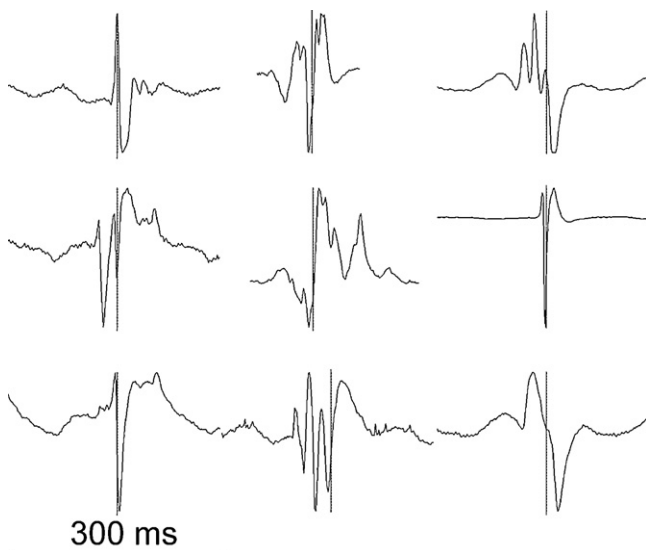
Fig. 2. Examples of patterns in the final library database. The vertical line indicates the actual activation time for each pattern that was determined by the expert analysts. The time interval t from pattern start to activation mark is the shift that is used to generate the estimated activation time when the template is optimally aligned with the input electrogram. All patterns have been scaled to the same peak-to-peak amplitude and plotted using the same time scale.

delay caused by low pass filtering during binary signal formation would not be expected to significantly affect the result. The process was repeated for all input electrograms, so that the correlation signal was obtained for each template, and the estimated activation time was selected from the template with the highest correlation maximum. Thus the template used to mark each electrogram could change from one cycle to the next.

2.4. Library database construction

To construct the database, a set of 350 templates were extracted from exemplar bipolar electrogram signals acquired using the 312 array during five instances of reentrant ventricular tachycardia in the canine postinfarction experiments (total of 1560 electrogram signals with recording duration of 5 s). The electrogram signals to be used as templates were selected as having varied shapes and multiphasic deflections. To increase computational efficiency, the library size was reduced prior to testing. When all 350 electrograms had been selected, each was cross-correlated with the other electrograms, and the electrograms with the highest average correlation value were removed from the set. The process was repeated until the database was reduced to a set of 120 electrograms that were mostly uncorrelated with one another. Of the 120 final template electrograms, the library size was adjusted subsequently to maximize sensitivity and positive predictive value (PPV) during subsequent testing of the algorithm. Examples from the library of 120 templates, along with their activation times as denoted by vertical lines, are shown in Fig. 2. There are a variety of shapes and multiphasic peaks, with differing amplitude and duration. Each pattern was stored along with its activation time t, which was determined by the expert analysts. Prior to storage, each pattern was normalized to 1 mV peak-to-peak amplitude.

2.5. Video animation

To animate the data, the location of each site was highlighted on a computerized electrode grid, and bilinear interpolation was used for aesthetic effect to extend the resolution of the map grid beyond the location of the 312 map points. The interpolation was done automatically in Matlab (ver. 5.1, 1997, The MathWorks, Inc., Natick, MA). For video animation, the output of the automated activation marking algorithm described above was smoothed in time to produce a fixed-width peak for each correlation maximum detected. Then, it was color-coded and its value was used to build each frame of the animation.

2.6. Measurement and statistics

To validate the automated marking process and the library set described above, electrogram recordings acquired from the canine epicardial border zone during pacing and reentrant ventricular tachycardia were marked for activation by the expert analysts. The automated algorithm was applied and the correspondence to manual marking was determined by tabulating the differences between manual and automated activation times. Activation time differences <10% of the maximum possible error, which depended on cycle length, were considered to be true positive (TP); otherwise the actual activation time that was not marked by the automated algorithm was classified as false negative (FN). Any time there was a mark made by the software with no corresponding mark by the user, it was considered to be a false positive (FP). There were no true negatives, since any position on the electrogram outside the 10% interval could be considered to be a true negative. Therefore only sensitivity S (true positives divided by true positives + false negatives) and positive predictive value PPV (true positives divided by true positives + false positives) were calculated. The sensitivity of
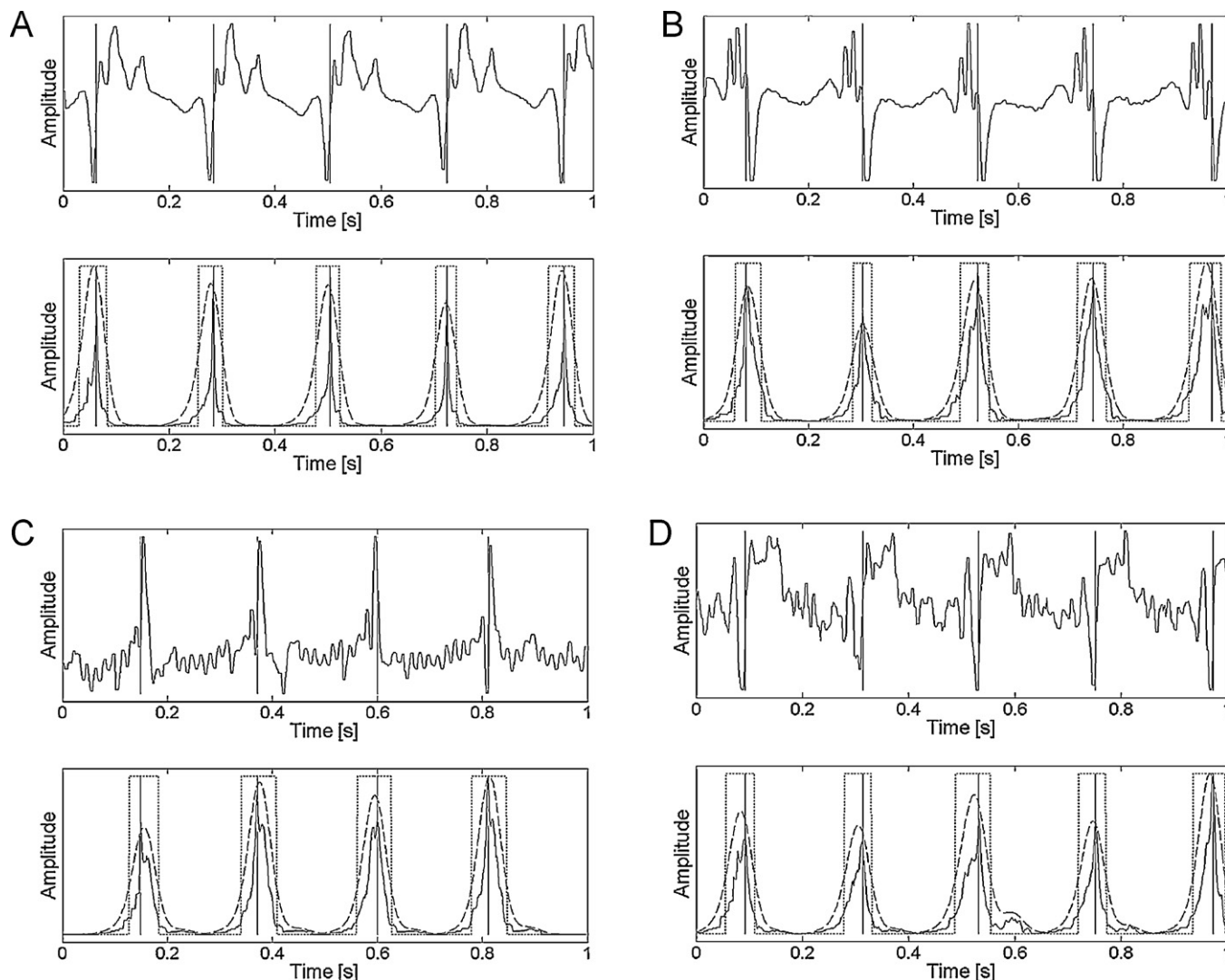
Fig. 3. Four electrograms (upper trace in panels A–D), and their unfiltered and filtered correlation signal with time window detected (lower traces in panels A–D). Each global maximum in the correlated signal indicates the estimated activation time.

the procedure was calculated as the percentage of beats correctly selected by the algorithm with respect to the total number of beats marked by the analyst. The positive predictive value was calculated as the percentage of beats correctly selected by the algorithm with respect to the total number of beats it detected. Results were presented as mean ± standard deviation.

3. Results

Fig. 3 shows the result of applying the algorithm to electrograms with additive noise over a 1 s analysis interval (4–5 cardiac cycles). In each panel, the input electrogram is in the upper panel, and in the lower panel is the correlation signal (solid line), the smoothed (filtered) correlation signal (dashed line), and the time windows detected after thresholding the smoothed correlation signal (dotted line). The electrograms in Fig. 3A and B have high signal-to-noise ratios but differ markedly in shape. Each electrogram is composed of multiple deflections with a relatively constant shape from one cycle to the next, except for some variation in amplitude. The electrogram in panel A has several wide deflections, whereas in panel B there are mostly narrow deflections. The correlation signals in the lower panels of Fig. 3A and B vary slightly in peak height. For both electrograms, each peak of the raw correlation aligns with

the region of sharpest slope associated with the largest deflection. The phase lag of the correlation signal has been adjusted by t, the actual activation time of the template (Fig. 3A and B – vertical lines). It is evident by comparison of the top and bottom panels in Fig. 3A and B that there is a close correspondence between manual and automated marking. Fig. 3C and D shows the result of applying the algorithm to two different electrograms with relatively low signal-to-noise ratio over the recording interval. Most of the noise is caused by 60 Hz frequency. Although noise is present, there is close correspondence between estimated and actual activation time. In panel C, the third beat was manually marked at the downward slope of the activation which is steepest on this cycle, instead of the upward slope as was done for beats 1, 2, and 4. The difference between estimated and actual activation time is still within ±5 ms.

Examples of automarking when electrograms have some cycle-to-cycle changes in morphology are shown in Fig. 4. The top panels show the electrogram and the bottom panels show the respective filtered correlation function. In the left top panel, changes in peak amplitude occur, particularly on the last cycle. In the right top panel, conduction alternans causes changes in the far-field signal. The automarking technique is robust to these types of alterations, which can be common in recorded electrograms.
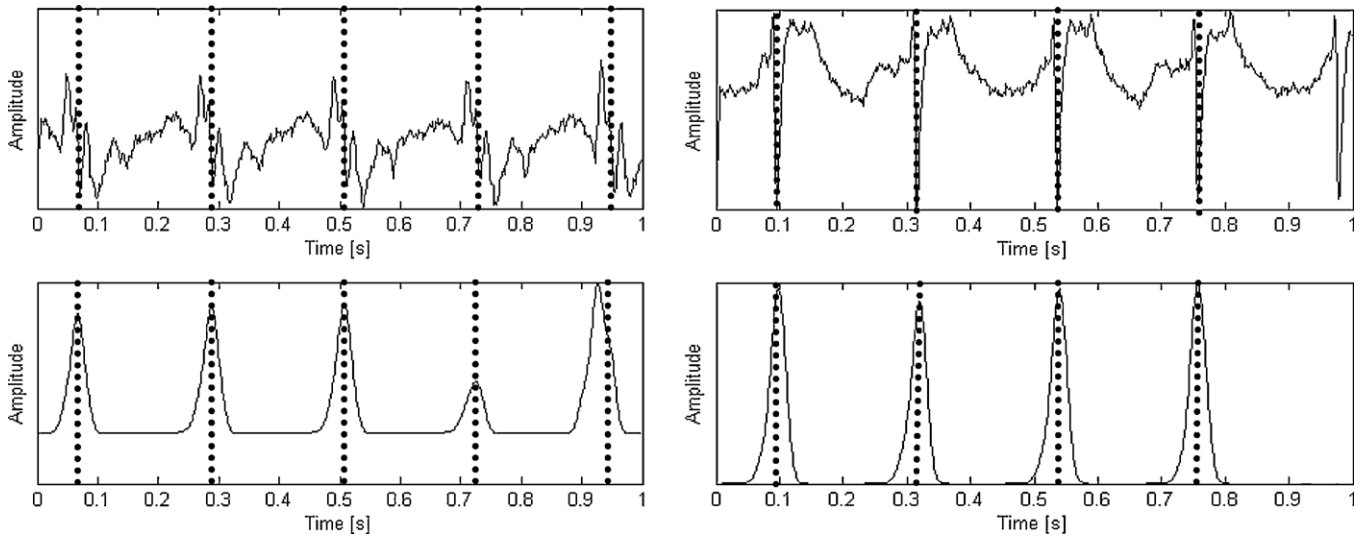
Fig. 4. Examples of electrograms with changing morphology (upper panels) and their filtered correlation signals (lower panels). The automarked location is shown as a vertical dashed line. For clarity the mask and unfiltered correlation signals are not shown.

The relationship between error function and correlation function for two electrogram series is shown in Fig. 5. This series was taken from the onset of monomorphic reentrant ventricular tachycardia with a double-loop circuit as initiated by premature excitation. The electrograms are shown in the top panels. The recording sites for the electrogram traces provided were in proximity to the reentry isthmus. The value of the template duration ℓ is 200 sample points. The raw correlation and error functions
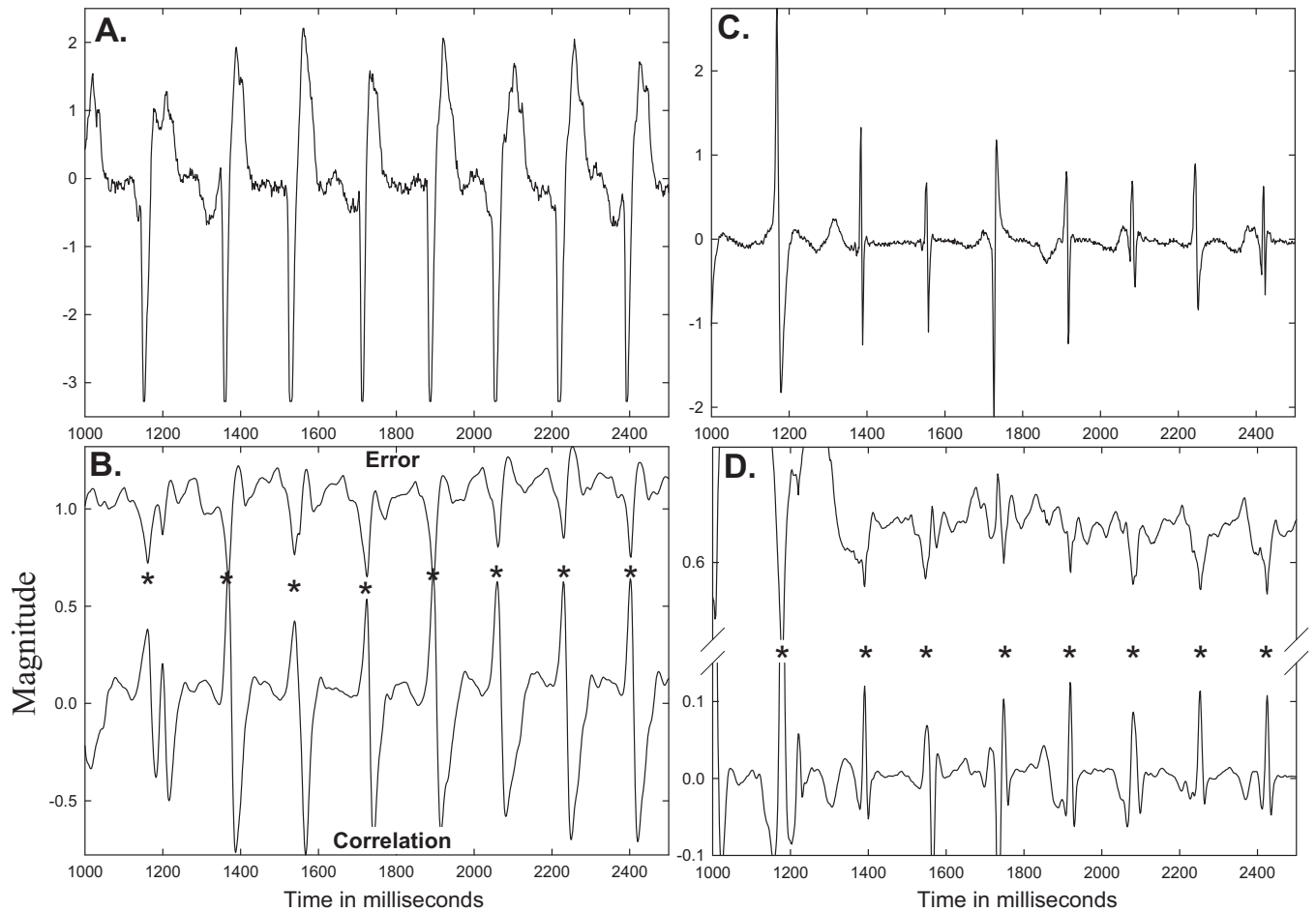
Fig. 5. Examples of automated electrogram marking at ventricular tachycardia onset. Panels A and C: Electrograms at onset; cycle length is approximately 180 ms. Panels B and D: Corresponding error function (upper trace) and correlation function (lower trace) for the electrograms of Panels A and C, respectively. Asterisks denote location of the automated activation mark for each cardiac cycle, which coincide within a few milliseconds to the sharpest slope in each electrogram deflection.
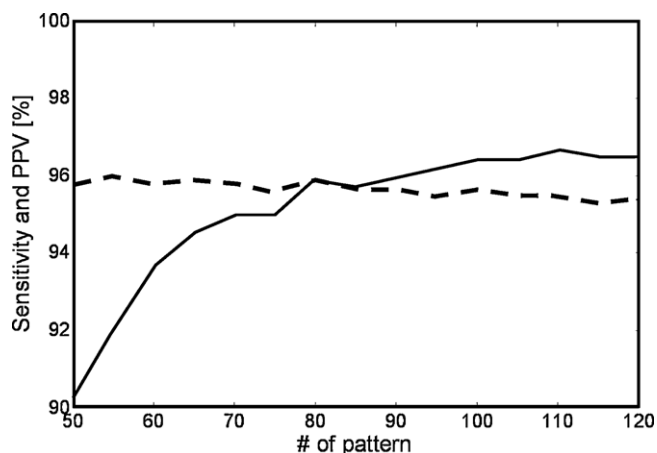
Fig. 6. Positive predictive value (dashed) and sensitivity (solid) for the method, using a library size from 50 to 120. The optimal number of patterns to be used in the template library is 80 (cross of traces).

Table 1
Statistics.

# pat.	Sensi.	PPV	TP	FP	FN
50	90.2	95.8	1354	59	147
60	93.5	95.8	1402	61	97
70	95.0	95.8	1423	62	75
80	95.9	95.9	1438	61	61
90	96.0	95.7	1436	64	60
100	96.4	95.7	1441	65	54
110	96.6	95.5	1441	68	51
120	96.5	95.4	1439	69	52

pat., number of patterns used for matching; sensi., sensitivity; PPV, positive predictive value; TP, true positives; FP, false positive; FN, false negatives. Total number of electrograms analyzed = 1560.

are graphed in the lower panels. Asterisks show the time of maximum/minimum in correlation and error function (max/min) each cardiac cycle. There is an alignment of max/min in the lower panels with the sharpest slope of each electrogram deflection in the top panels, which is the actual activation time. Although some of the electrograms are quite variable in morphology from one cardiac cycle to the next, the alignment error is at most a few milliseconds.

The relationship between varying library database size from 50 to 120 template patterns, to the sensitivity and PPV statistics as applied to the exemplar set of 1560 electrograms, is shown in Fig. 6 (solid and dashed lines, respectively). The sensitivity sharply decreases as the database size decreases below 80 templates. The PPV decreases slightly when more than 80 templates are included in the library database. The statistics of Fig. 6 are displayed in Table 1 for increments of 10 patterns. At left are shown the sensitivity and positive predictive values, and at right are the number of true positives, false positives, and false negatives out of a total of 1560 electrograms analyzed. Most analyzed electrograms were correctly marked by automated means even when only 50 patterns

were used (≥1354 electrograms). In many instances the number of false positives (incorrect markings) and false negatives (not marked where an activation event occurred) was only a small fraction of the total number of electrograms analyzed. However at 50–60 patterns used for matching, the number of false negatives was relatively high (147 and 97, respectively) due to the smaller template pool, which caused some deflections to not be recognized as an activation event.

A database size of 80 templates resulted in a sensitivity and PPV greater than 95%, and this value was used to estimate activation time in the test set. For all test set data, the automated marking process had a sensitivity of 95.9% and a PPV of 83.8%. The mean difference in time between estimated and actual activation marks was 2.1 ± 3.9 ms. Each activation marking analysis of 312 electrograms required approximately 10 s to complete prior to display of the video on a fast PC-type computer.

An example of an automatically generated isochronal activation map of the left ventricular epicardial border zone during induction of double-loop reentrant ventricular tachycardia is shown in Fig. 7. Stimulation from the LAD margin with the right ventricle at a 300 ms overdrive coupling interval resulted in induction of this tachycardia. The activation map without error function correction is shown in Fig. 7A. The interval for activation of the entire mapped area following the stimulus is approximately 160 ms, and the sequence of activation is shown by the isochrones. Activation proceeds rapidly from the pace site toward the center of the
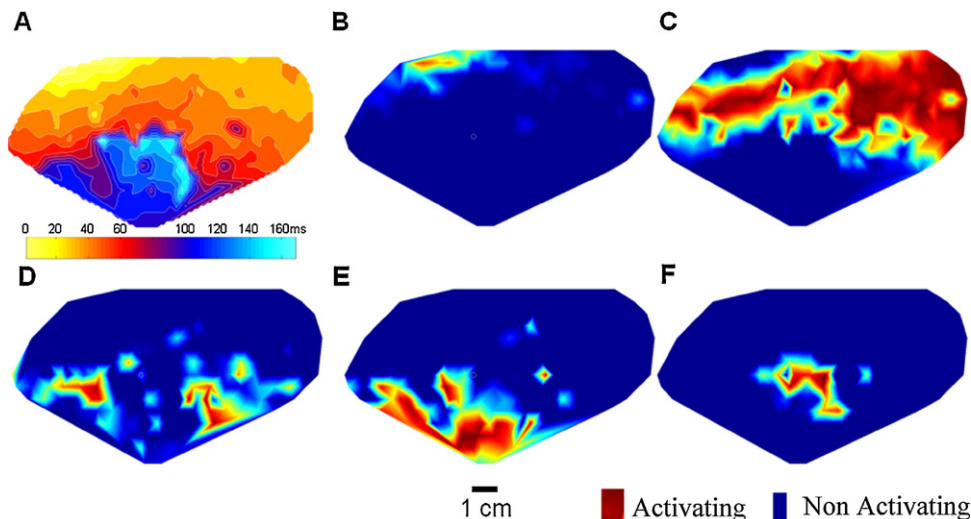
Fig. 7. Estimated activation times during extrastimulation from the left anterior descending coronary artery pacing site. (A) Contour map without error function correction. (B–F) Five images taken from an animation sequence generated by the algorithm with error function correction. The contribution of the several noisy electrograms with incongruous activation times (panel A) were excluded during the automated constructing of the animation maps (panels B–F). Images are separated by 32 ms (the entire area activates in 160 ms). Regions of dark orange-red are activating during the time epoch of the map. Generation of the colormap for panels B–F is described in the text. (For interpretation of the references to color in this figure legend, the reader is referred to the web version of the article.)
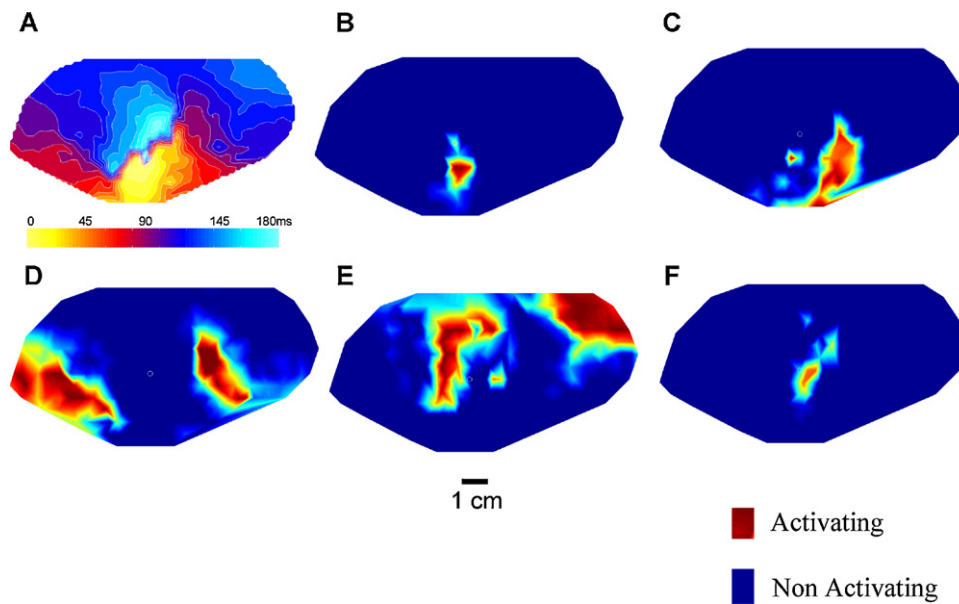
Fig. 8. Estimated activation times during sustained reentrant ventricular tachycardia. (A) Contour map. (B–F) Five images taken from the animation sequence generated by the algorithm. Images are separated by 40 ms. Areas of dark orange-red are activating. (For interpretation of the references to color in this figure legend, the reader is referred to the web version of the article.)

grid (upper left in Fig. 7A, yellow). Functional conduction block occurs near the center due to refractoriness, so that the wavefront bifurcates, the distinct wavefronts curve around, and then they coalesce toward the lower portion of the mapping gird (apical-LAT margin). There is a pause in conduction (light blue) which was followed by reentry into the previously excited border zone region, so that ventricular tachycardia onset occurs. Examples of animation maps for this cardiac cycle are shown in Figs. 7B–F, and they represent the same activation sequence as is shown by the activation map in Fig. 7A. However the colors in Fig. 7B–F are representative of activation status, not activation time as in panel A. In Fig. 7B–F, red denotes the occurrence of activation, while blue indicates that there is no activation during the particular time epoch of the frame. Yellow represents border areas between activation and non-activation. The stimulus site corresponds approximately to the small red region at upper left in panel B, at the LAD margin with the right ventricle, and the wavefront begins to expand outward (yellow). In panel C, a large area of the border zone is activating, and conduction velocity is rapid. However, the wavefront encounters an obstacle in panel D and bifurcates. The distinct wavefronts continue in the same direction, toward the apical-LAT margin which is toward the bottom of the grid. Coalescence of the wavefronts is shown in panel E to occur at the apical-LAT margin. The solitary wavefront then proceeds through a constrained region (panel F), and then reenters the previously excited tissue in the direction toward the LAD margin.

Animation for a cycle of sustained reentrant ventricular tachycardia after its induction by extrastimulation is shown in Fig. 8 and it is from a different experiment than Fig. 7. The panels show an activation map (A) and the animation sequence (B–F). The reentrant circuit present in the epicardial border zone (A) had a cycle length of 180 ms for the cycle shown. Panels B–F show selected time epochs of the animation map. Late diastolic activation is shown in panel B, exit of the activation wavefront from the isthmus in panel C, propagation as two distinct wavefronts around the periphery in panels D–E, and coalescence at the isthmus entrance in panel F. Exit from the isthmus is toward the apical-LAT margin in Fig. 8F.

4. Discussion

4.1. Algorithm

An algorithm for automated marking and mapping of electrograms acquired from the epicardial border zone during ventricular tachycardia in canine postinfarction was described. The correlation and error functions were used for marking, and they can easily be adjusted to change the desired sensitivity and PPV of the detection algorithm if needed. The dynamic and beat-to-beat variability of electrogram waveforms over time during ventricular tachycardia can be significant. Thus the ability of the algorithm to switch templates for marking (see Section 2), or even to develop a new set of library templates when new types of electrogram data arise, can be helpful to increase the robustness of the approach. In our study, for signals with low signal-to-noise ratio, most of the misdetections in the test set were due to unexpected activation patterns that were not included in the database. To resolve this problem in future versions of the algorithm, the database can be continuously updated using a self-learning system with weighted adaptation [22,23]. For signals with poor signal-to-noise ratios, peaks in the correlation signal sometimes aligned with an electrogram's sharpest noisy waves, while the true activation point was partially masked by noise and remained undetected. A notched or matched filter to remove frequencies near 60 Hz can be incorporated in future versions of the algorithm in cases when line frequency interference is significant.

4.2. Other automated activation marking and mapping techniques

When reentrant ventricular tachycardia originates from the infarct border zone, the extracellular signal shape is complex and the contribution of far-field potentials can be substantial [23]. For automated detection of complex electrogram activation time, morphologically based algorithms such as is described in our study have been shown to be advantageous as compared with slope-and peak-based methods [24]. Morphologically based algorithms have also been found useful to quantify electrogram organization

during atrial fibrillation, and to distinguish between different episodes of atrial fibrillation [25]. A reconstruction of the passage of the electrical wavefront can be developed by modeling electrogram morphology as a symmetrical biphasic shape that neglects far-field activation and electrode diameter [26]. Activation time is then estimated using deconvolution. Areas of electrical conduction block have been automatically detected from time-frequency analysis of unipolar electrograms [27]. Bipolar electrograms, used in our study, may be more difficult to analyze via spectral methods, since deflections tend to be sharper and more complex. Methods for automated detection of spatiotemporal features in activation maps have been developed by extracting wavefront structure from epicardial data using graphical techniques [13]. Such higher-level information would be useful to incorporate into our paradigm to determine, for example, the location of ectopic sites and abnormal propagation regions. Automatic marking and mapping of human atrial fibrillation has been done using a template library of mathematically defined unipolar electrograms [12]. However, complex fractionated atrial electrogram components can be difficult to match and required separate analysis. The simultaneous use of correlation and error functions to determine the global optimum, as described in our study, may improve robustness to identify complex fractionated atrial electrogram activation times even though these waveforms are multiphasic, because points of high correlation must coincide with points of low error difference for there to be a match (see Fig. 5).

4.3. Limitations

Errors can arise when activation times are assigned at recording sites where local electrical activity at the site does not occur and only far-field deflections are recorded. To account for this possibility, another level of complexity, in the form of inclusion of spatial relationships, could be added to future versions of the automated implementation. The algorithm was developed and tested with a small number of experiments. These results should be confirmed using a larger number of test sets. The automated marking algorithm diminished in accuracy in the presence of 60 Hz noise, which should be removed by notch or matched filtering in subsequent versions. For isochronal mapping, the stimulus artifact can be a very important source of misdetection of the activation time, and should be masked when stimulus wavefronts are mapped. Application to unipolar electrograms, which may have subtle deflections due to local electrical activity, should be tested in future study. The automarking algorithm was also not tested under fibrillatory conditions, where estimation of activation time can be greatly affected by electrogram fractionation. The applicability of the method under these conditions should be determined in future work.

5. Conclusion

An automated algorithm was developed to mark the electric activation time of bipolar electrograms recorded from the epicardial surface in postinfaction canine hearts. The algorithm was shown to be useful for rapid and accurate automatic marking of multichannel electrograms, many of which were complex, during ventricular tachycardia caused by a reentrant circuit. Based on the activation marks, display of sequential color activation maps and their usefulness to track the activation wavefront was shown.

Conflicts of interest

All of the authors have no conflicts of interest to report.

Acknowledgments

References

[1] P.W. Hsia, L. Fendelander, G. Harrington, Damiano RJ, Defibrillation success is associated with myocardial organization. Spatial coherence as a new method of quantifying the electrical organization of the heart, Journal of Electrocardiology 29 (Suppl.) (1996) 189–197.

[2] X.H. Wehrens, S.E. Lehnart, S.R. Reiken, S.X. Deng, J.A. Vest, D. Cervantes, J. Coromilas, D.W. Landry, A.R. Marks, Protection from cardiac arrhythmia through ryanodine receptor-stabilizing protein calstabin2, Science 304 (2004) 292–296.

[3] D. Panescu, Intraventricular electrogram mapping and radiofrequency cardiac ablation for ventricular tachycardia, Physiological Measurement 18 (1997) 1–38.

[4] Y.H. He, R.N. Ghanem, A.L. Waldo, Y. Rudy, An interactive graphical system for automated mapping and display of cardiac rhythms, Journal of Electrocardiology 32 (1999) 225–241.

[5] P. Della Bella, S. Riva, Hybrid therapies for ventricular arrhythmias, Pacing and Clinical Electrophysiology 29 (Suppl. 2) (2006) S40–S47.

[6] A.L. Wit, Ablation of ventricular tachycardia does anyone have any new ideas, Heart Rhythm 3 (2006) 198–200.

[7] O.R. Segal, A.W. Chow, V. Markides, R.J. Schilling, N.S. Peters, D.W. Davies, Long-term results after ablation of infarct-related ventricular tachycardia, Heart Rhythm 2 (2005) 474–482.

[8] J.T. Jacobson, V.X. Afonso, G. Eisenman, J.R. Schultz, S. Lazar, J.J. Michele, M.E. Josephson, D.J. Callans, Characterization of the infarct substrate and ventricular tachycardia circuits with noncontact unipolar mapping in a porcine model of myocardial infarction, Heart Rhythm 3 (2006) 189–197.

[9] G.D. Clifford, F. Azuaje, McSharry PE (Eds.), Advanced Methods and Tools for ECG Data Analysis, Artech, House, Boston/London, 2006, pp. 300–384.

[10] V. Krasteva, I. Jekova, QRS template matching for recognition of ventricular ectopic beats, Annals of Biomedical Engineering 35 (2007) 2065–2076.

[11] R.E. Ideker, W.M. Smith, S.M. Blanchard, S.L. Reiser, E.V. Simpson, P.D. Wolf, N.D. Danieley, The assumptions of isochronal cardiac mapping, Pacing and Clinical Electrophysiology 12 (1989) 456–478.

[12] R.P. Houben, M.A. Allessie, Processing of intracardiac electrograms in atrial fibrillation. Diagnosis of electropathological substrate of AF, IEEE Engineering in Medicine and Biology Magazine 25 (2006) 40–51.

[13] R.P. Houben, N.M. de Groot, F.W. Lindemans, M.A. Allessie, Automatic mapping of human atrial fibrillation by template matching, Heart Rhythm 3 (2006) 1221–1228.

[14] P.I. Gardner, P.C. Ursell, J.J. Fenoglio Jr., A.L. Wit, Electrophysiologic and anatomic basis for fractionated electrograms recorded from healed myocardial infarcts, Circulation 72 (1985) 596–611.

[15] S.M. Dillon, M.A. Allessie, P.C. Ursell, A.L. Wit, Influences of anisotropic tissue structure on reentrant circuits in the epicardial border zone of subacute canine infarcts, Circulation Research 63 (1988) 182–206.

[16] E.J. Ciaccio, A.E. Saltman, O.M. Hernandez, R.J. Bornholdt, J. Coromilas, Multi-channel data acquisition system for mapping the electrical activity of the heart, Pacing and Clinical Electrophysiology 28 (2005) 826–838.

[17] M.A. Langston, C.F. Pieper, A. Pacifico, Spectral analysis of activation time sequences, Pacing and Clinical Electrophysiology 17 (1994) 1288–1299.

[18] E.J. Ciaccio, Localization of the slow conduction zone during reentrant ventricular tachycardia, Circulation 102 (2000) 464–469.

[19] E.J. Ciaccio, A.W. Chow, D.W. Davies, A.L. Wit, N.S. Peters, Localization of the isthmus in reentrant circuits by analysis of electrograms derived from clinical noncontact mapping during sinus rhythm and ventricular tachycardia, Journal of Cardiovascular Electrophysiology 15 (2004) 27–36.

[20] A. Ambardar, Analog and Digital Signal Processing, PWS Pub, Co., 1995, pp. 1–253.

[21] J.G. Proakis, D.G. Manolakis, Digital Signal Processing. Principles, Algorithms and Applications, 3rd ed., Prentice-Hall, Inc., 1996, pp. 1–68.

[22] E.F. Treo, M.C. Herrera, M.E. Valentinuzzi, Algorithm for identifying and separating beats from arterial pulse records, BioMedical Engineering Online 4 (2005) 48.

[23] E.J. Ciaccio, M.M. Scheinman, V. Fridman, H. Schmitt, J. Coromilas, A.L. Wit, Dynamic changes in electrogram morphology at functional lines of block in reentrant circuits during ventricular tachycardia in the infarcted canine heart a new method to localize reentrant circuits from electrogram features using

adaptive template matching, Journal of Cardiovascular Electrophysiology 10 (1999) 194–213.

[24] C.F. Pieper, R. Blue, A. Pacifico, Simultaneously collected monopolar and discrete bipolar electrograms comparison of activation time detection algorithms, Pacing and Clinical Electrophysiology 16 (1993) 426–433.

[25] L. Faes, G. Nollo, R. Antolini, F. Gaita, F. Ravelli, A method for quantifying atrial fibrillation organization based on wave morphology similarity, IEEE Transactions on Biomedical Engineering 49 (2002) 1504–1513.

[26] W.S. Ellis, S.J. Eisenberg, D.M. Auslander, M.W. Dae, A. Zakhor, M.D. Lesh, Deconvolution a novel signal processing approach for determining activation time from fractionated electrograms and detecting infarcted tissue, Circulation 94 (1996) 2633–2640.

[27] F.G. Evans, J.M. Rogers, W.M. Smith, R.E. Ideker, Automatic detection of conduction block based on time-frequency analysis of unipolar electrograms, IEEE Transactions on Biomedical Engineering 46 (1999) 1090–1097.